

HAPTICS

Full freedom-of-motion actuators as advanced haptic interfaces

Kyoung-Ho Ha^{1†}, Jaeyoung Yoo^{1,2†}, Shupeng Li^{3†}, Yuxuan Mao^{3,4}, Shengwei Xu³, Hongyuan Qi³, Hanbing Wu³, Chengye Fan³, Hanyin Yuan³, Jin-Tae Kim^{1,5}, Matthew T. Flavin^{1,6}, Seonggwang Yoo^{1,7}, Pratyush Sahrir⁸, Sangjun Kim⁹, Hak-Young Ahn¹, Edward Colgate³, Yonggang Huang^{3,10,11*}, John A. Rogers^{1,3,8,11,12*}

The sense of touch conveys critical environmental information, facilitating object recognition, manipulation, and social interaction, and can be engineered through haptic actuators that stimulate cutaneous receptors. An unfulfilled challenge lies in haptic interface technologies that can engage all the various mechanoreceptors in a programmable, spatiotemporal fashion across large areas of the body. Here, we introduce a small-scale actuator technology that can impart omnidirectional, superimposable, dynamic forces to the surface of skin, as the basis for stimulating individual classes of mechanoreceptors or selected combinations of them. High-bit haptic information transfer and realistic virtual tactile sensations are possible, as illustrated through human subject perception studies in extended reality applications that include advanced hand navigation, realistic texture reproduction, and sensory substitution for music perception.

The sense of touch conveys essential information about the physical environment, with critical roles in identifying and manipulating objects and in strengthening social interactions. Sensations arise from mechanical stimulation of cutaneous receptors that consist of specialized dendritic endings of afferent nerve fibers. These mechanoreceptors exist in complex distributions deep into the skin and across all regions of the body (1). Recent research focuses on the development of engineered systems that are capable of creating tactile sensations through these mechanisms in a fast, programmable manner with devices in thin, flexible formats that can interface with small or large areas of the skin, not limited to the fingertips (2–5). When combined with well-developed systems for visual and auditory inputs, such technologies can qualitatively enhance immersive experiences in extended reality (XR) environments, for applications that

span entertainment, social media, medicine, and physical rehabilitation (6, 7). The integration of sensors with these actuators offers the potential to provide closed-loop feedback for teleoperations (8, 9) and remote health care (10). Specific opportunities include applications for amputees and those with visual or hearing impairments, where engagement with the somatosensory system can substitute and augment diminished natural capabilities for sensing (11, 12).

The effectiveness of these systems depends on accurately reproducing the complex spatiotemporal patterns of activation of mechanoreceptors during the broad range of mechanical deformations that result from the natural processes of touch. Each of the four classes of mechanoreceptors that innervate various regions of the skin (13) responds to forces with specific combinations of directionality, magnitude, and frequency (Fig. 1A) (14–16). These receptors trigger action potentials with different timing responses to mechanical stimuli based on their rates of adaptation. The resulting pulses pass through sensory neurons to the brain to create distinct perceptions (17, 18). Some schemes aim to generate programmable multidirectional forces on the skin by strategically arranging multiple types of actuators, including those based on electromagnetic motors (19–21), pneumatic systems (22, 23), shape-memory alloys (24, 25), and electrostatic assemblies (26). These approaches, however, have characteristics that are not ideally suited for immersive XR experiences owing to some combination of disadvantages in their relatively large sizes and masses, limited options in attachment locations, difficulty in distributing into programmable arrays, challenges in balancing requirements in forces and displacement distances, inability to achieve superimposable

modes of actuation, and constraints in operating speeds and frequencies (table S1).

Freedom-of-motion actuators

Here, we introduce a wireless, real-time haptic interface with full freedom of motion in generating programmable deformations at the surface of the skin. This engineering capability can reproduce the span of displacements and forces, both in magnitude and direction, necessary to engage all receptors in the skin in a targeted manner. Each actuator uses a collection of individually addressable wire coils to generate magnetic fields with user-defined directions and magnitudes. Lorentz forces produced by interaction with one or more fixed magnets that interface to the skin serve as the basis for operation. Figure 1A illustrates normal, shear, torsional, and vibrational stimuli that can be produced using this approach, through corresponding calculations of distributions of strain across the surface of the skin and into its depth. Normal forces stimulate three types of mechanoreceptors under specific conditions: Merkel cells respond to static forces with a small threshold, while Meissner and Pacinian corpuscles respond to low- and high-frequency vibrations, respectively. Stretching of the skin induced by shear or torsional motions activates Ruffini endings (14). The superposition of forces generated with a single actuator unit, which we refer to as a freedom-of-motion (FOM) actuator, can address a physiologically relevant range of magnitudes and time dynamics to engage each of these mechanoreceptors individually or in combination.

Figure 1B shows some details of the simplest form of actuator that uses these design principles, together with a sensor that enables advanced mechanisms for control. Two rectangular solenoid coils of different dimensions enable one (shear-x) to be inserted orthogonally into the other (shear-y). Yet another coil, a short round solenoid (normal-z), inserts into the shear-x coil, resulting in a nested tri-coil assembly. A solid lubricating film serves as a low-friction interface that laminates beneath these coils, secured by a structure with supporting legs that can be customized in shape and materials on the basis of requirements for interfacing the FOM actuator with various regions of the skin. The end effector consists of a rectangular neodymium magnet positioned beneath the coils with a small air gap in between, coupled to the epidermis using a thin, compliant adhesive. An arm structure extends from the magnet in four orthogonal horizontal directions to ensure pure shear motions upon application of suitable currents through the shear-x and shear-y coils, by inhibiting out-of-plane torsional rotations (fig. S1). An inertial measurement unit (IMU) placed above the coils senses the egocentric coordinates and motion of the specific body part, as a reference for application of directional adaptive haptic stimuli.

¹Querrey-Simpson Institute for Bioelectronics, Northwestern University, Evanston, IL, USA. ²Department of Semiconductor Convergence Engineering, Sungkyunkwan University, Suwon, Republic of Korea. ³Department of Mechanical Engineering, Northwestern University, Evanston, IL, USA. ⁴Institute of Biomedical Manufacturing and Life Quality Engineering, School of Mechanical Engineering, Shanghai Jiao Tong University, Shanghai, China. ⁵Department of Mechanical Engineering, Pohang University of Science and Technology, Pohang, Republic of Korea. ⁶School of Electrical Engineering and Computer Engineering, Georgia Institute of Technology, Atlanta, GA, USA. ⁷College of Biomedical Science and Health, Inje University, Gimhae, Republic of Korea. ⁸Biomedical Engineering, Northwestern University, Evanston, IL, USA. ⁹Department of Mechanical Engineering, University of Texas at Austin, Austin, TX, USA. ¹⁰Department of Civil and Environmental Engineering, Northwestern University, Evanston, IL, USA. ¹¹Department of Materials Science and Engineering, Northwestern University, Evanston, IL, USA. ¹²Department of Neurological Surgery, Feinberg School of Medicine, Northwestern University, Chicago, IL, USA. *Corresponding author. Email: y-huang@northwestern.edu (Y.H.); jrogers@northwestern.edu (J.A.R.)
†These authors contributed equally to this work.

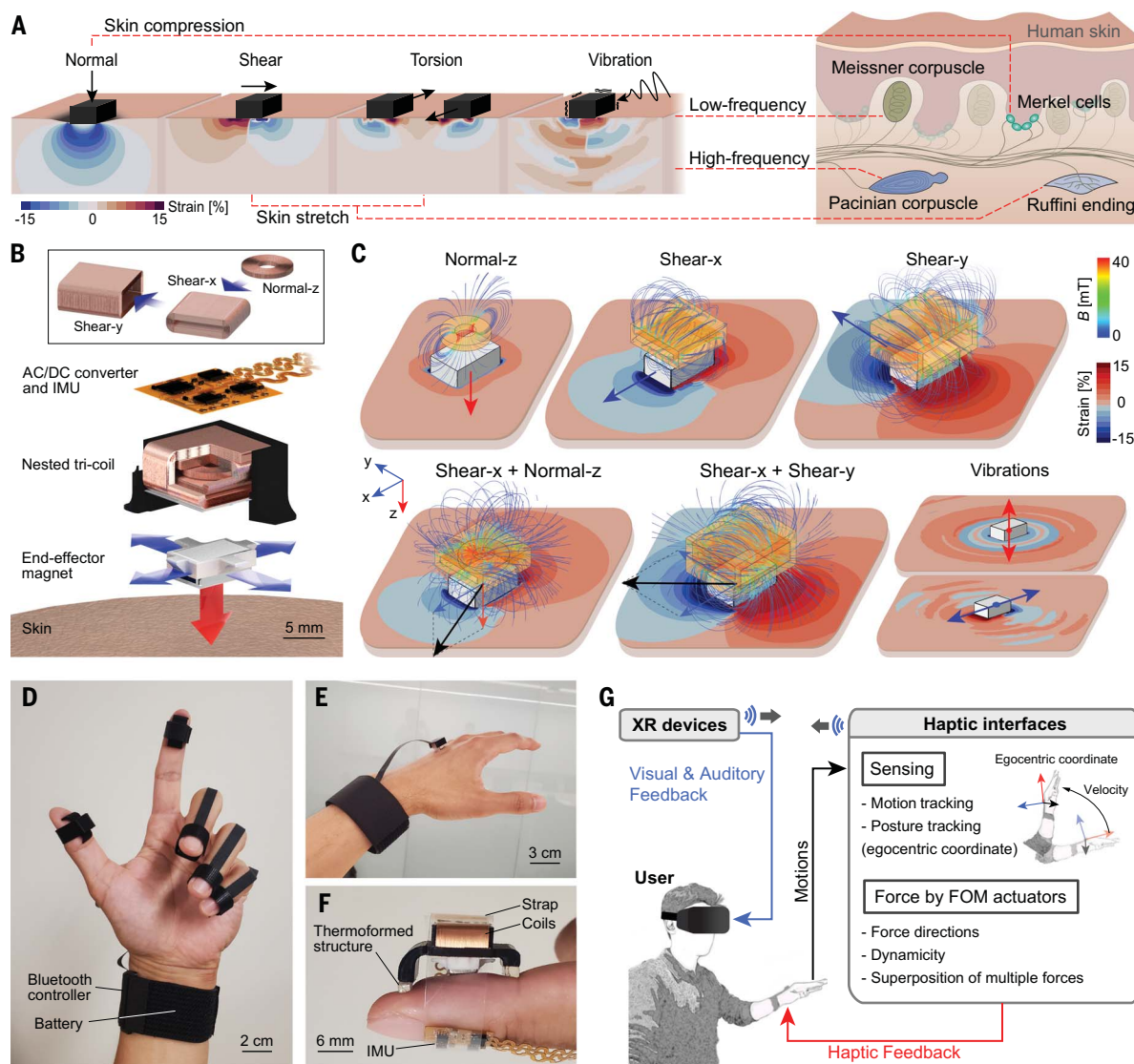


Fig. 1. Multisensory haptic interfaces with a full FOM actuator. (A) Various modes of mechanical stimuli and corresponding strain fields simulated for human skin. Diagram on the right shows the four main mechanoreceptors in the skin and their responses to distinct mechanical stimuli. (B) Disassembled view of the FOM actuator, with an IMU to enhance control methodologies. The inset shows an assembly of three coils into the nested tri-coil assembly. (C) Operating principles of the FOM actuator, illustrating the magnetic fields produced by current passing through the coils and the corresponding electromagnetic forces

on the magnetic end effector. Simulated distributions of strain and their time-dependent propagation on and in the skin. (D) Photograph of the FOM actuators mounted on the fingertips, with a wireless control unit and battery in a wrist band. (E) Photograph of an FOM actuator mounted on the dorsal hand. (F) Photograph of a skin-integrated FOM actuator on a fingertip facilitated by a conformable thermoforming interface and a transparent strap. (G) State diagram that illustrates the use of wireless, battery-powered FOM actuator with integrated IMU in an XR environment.

Figure 1C illustrates the magnetic fields generated by passing current through the different coils, the resulting movements of the magnet, and the corresponding distributions of strains and propagation of them in the skin, for representative modes of mechanical stimulus. The normal-z coil can induce forces in the out-of-plane direction (relative to the surface of the skin), whereas the shear-x and shear-y coils can generate tangential forces in the two in-plane directions. Simultaneously operating these coils yields a sum of the individual orthogonal force vectors, thereby enabling omnidirectional forms of programmable actuation.

Referring to the skin deformations in Fig. 1, A and C, normal force induces compressive strain deep within the skin rather than spreading laterally. Conversely, shear forces cause shallow, widespread deformations, with compressive strain in the forward direction and tensile strain in the rear. Vibrational stimuli, achieved by applying alternating current to the coils, produce waves of propagation into the depth and along the surface of the skin, with both longitudinal and shear content and varying waveforms depending on the direction of the vibrations.

The FOM actuator and sensor assembly, each equipped with a suitable mounting framework, can be positioned on nearly any body part, with wireless connectivity through a compact Bluetooth low-energy (BLE) electronic system and a small rechargeable battery (Fig. 1, D and E, and figs. S2 and S3). The result allows coordinated wireless operation in an array format or individually through a graphical user interface on a BLE-enabled external device. The photograph in Fig. 1F provides a magnified side view that shows a thermoformed soft structure and a strap to facilitate contact to curved surfaces of

the skin, as a robust but comfortable interface. Skin-integrated single or multiple FOM actuators with sensors can provide realistic sensations or haptic information for various XR applications, referenced to real-time motions of the human body, in wireless coordination with portable XR devices, such as smart glasses, virtual reality headsets, and smartphones (Fig. 1G).

Design principles and characterization

Optimal designs to allow miniaturization of these concepts in power-efficient actuators require careful consideration of the direction and magnitude of forces and the displace-

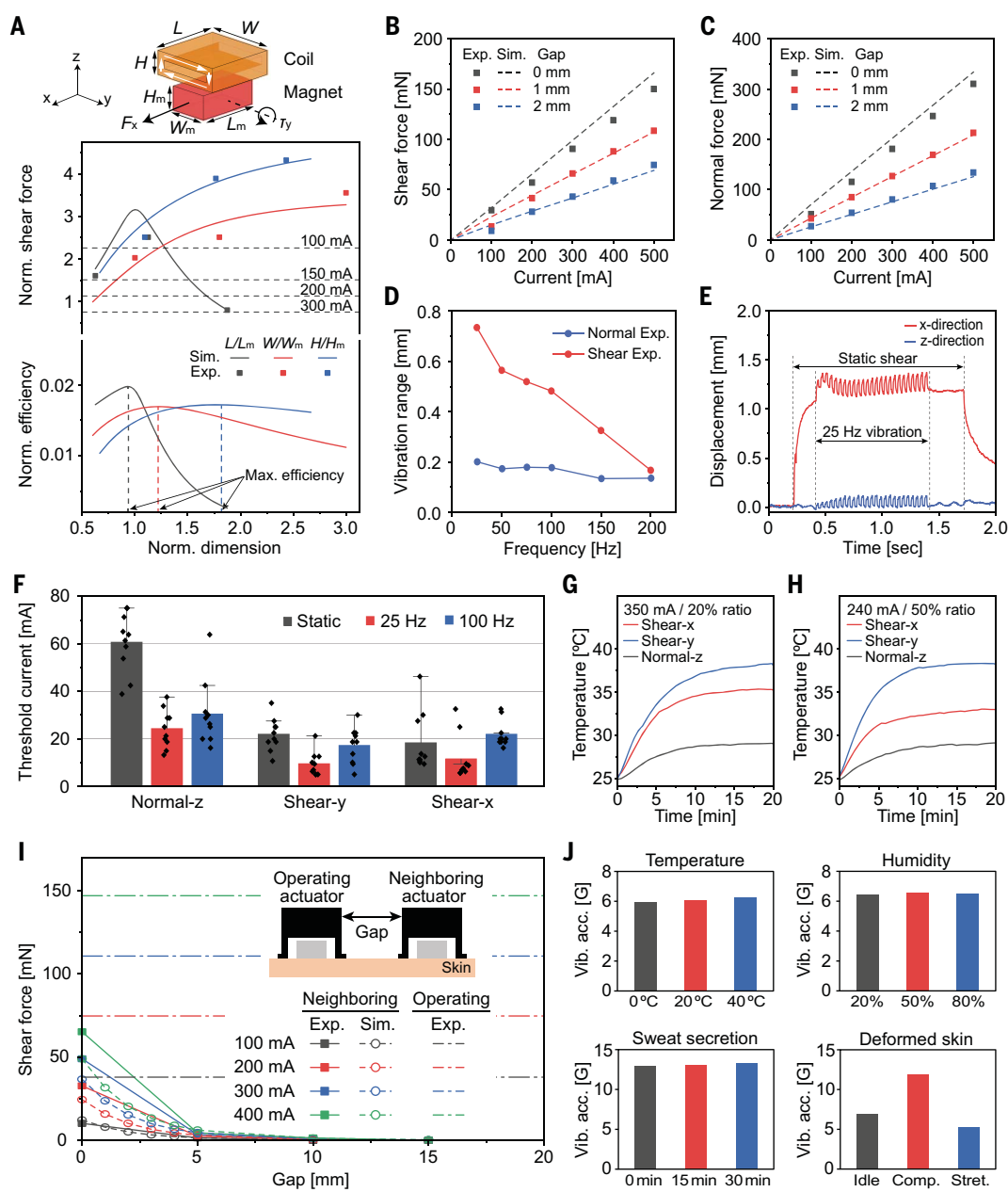
ments necessary for reliable human perception. Figure 2A and fig. S4 present an experimentally validated parametric analytical model that calculates a nondimensional (normalized) force and power efficiency metric, incorporating variables such as applied current, type of magnet, coil filling factor, and wire diameters. The analytical model evaluates the impact of each coil dimension individually with other parameters held constant (table S2).

The force generated by the normal-z coil, used exclusively in standard electromagnetic actuators (4, 27–29), increases with its outer diameter and thickness of the coil and decreases with its inner diameter (fig. S4). The

power efficiency, however, depends on the coil dimensions relative to those of the magnet, with a maximum when the outer radius is 1.4 times the effective radius of the magnet ($R/R_m = 1.4$), while monotonically decreasing with coil height. In the given coil dimensions and filling factor, force decreases, while efficiency linearly increases with the square of the wire diameter (see supplementary text in the supplementary materials).

Directional shear and torsional forces result from the shear-x and shear-y coils and their coordinated operation. As with the normal-z coil, the performance of these shear coils depends on their dimensions relative to those of

Fig. 2. Design strategies and characteristics of multimodal actuators by experiment and simulation. (A) Dimensional parametric analysis of the shear coil on force and efficiency. Parallel dashed lines indicate the threshold shear force, which are perceivable forces on human skin (2 kPa) at various operating currents. (B) Shear force as a function of the current and the gap between the shear coil and magnet. (C) Normal force as a function of the current and the gap between the normal coil and magnet. (D) Dynamic range of normal and shear vibrations depending on the frequency. (E) Simultaneous actuation of shear and normal coils to generate static shear force and 25 Hz of vibration. (F) Amplitude thresholds of human perception for the nested tri-coil FOM actuators across multiple modes (normal-z, shear-y, shear-x) and frequencies (static, 25 Hz, 100 Hz). (G) Temperature of the FOM actuator with a 20% duty cycle at 350 mA on each coil. (H) Temperature of the FOM actuator with a 50% duty cycle at 240 mA on each coil. (I) Interfering shear forces in neighboring actuators at various gap sizes compared with the shear forces on the operating actuator. The inset illustration depicts the definition of the gap. (J) Effects of environmental conditions on the performance of the FOM actuator (vibrational acceleration of the FOM actuator magnet, operated at 100 Hz and 100 mA): temperature, humidity, sweat secretion, and skin deformation (15% compression and 15% stretch).



the magnet (Fig. 2A). The shear force reaches its peak value when the coil length equals the magnet length ($L/L_m = 1$) and monotonically increases with both the width and height of the coil. The horizontal dashed lines in Fig. 2A denote design requirements for generation of perceivable stress (30) at operating currents ranging from 100 to 300 mA. The coil efficiency has an optimum value when the ratios of length (L/L_m), width (W/W_m), and height (H/H_m) are 0.93, 1.24, and 1.8, respectively. Additionally, similar lengths for the coil and magnet ($L/L_m = 0.96$) prevent unintentional torsional forces on the magnet during shear operations (fig. S5). For a wire diameter of 114 μm , and an N55 neodymium magnet, with $L/L_m \sim 1$ and with values of W and H that facilitate construction of the nested tri-coil assembly, optimal choices for the dimensions of the inner and outer shear coils are $L/L_m = 1.13$, $W/W_m = 1.8$, and $H/H_m = 1.09$ and $L/L_m = 1.14$, $W/W_m = 2.22$, and $H/H_m = 1.96$, respectively. The dimensions of the normal-z coil, with 79- μm -diameter wire, maximize its size within the available space constraints of the nested tri-coil assembly, specifically $D_{\text{out}} = 7$ mm, $D_{\text{in}} = 3$ mm, and $H = 0.9$ mm (fig. S6). The complete dimensions of an FOM actuator with these designs are 11.7 mm by 10.8 mm by 8.4 mm, and its weight are 3.19 g, including an 8 mm by 5 mm by 3 mm magnet and a packaging structure. Per simulation estimates, the size of the FOM actuator can be reduced to 5 mm by 5 mm by 3.5 mm while still generating human-perceivable normal and shear stress (2 kPa), under the given conditions of commercially available wire (0.079 μm diameter), a neodymium magnet, and operational currents up to 500 mA.

The operating parameters and the assembly structure, of course, also influence the dynamics of the system. Specifically, shear and normal forces linearly increase with the currents in the coils and nonlinearly decrease with the gap between coil and magnet (Fig. 2, B and C). Compared with the vertical distance (gap), the horizontal center-to-center distance causes a smaller reduction in forces (fig. S7). The chosen gap between the outermost coil and the magnet is 0.2 mm, as a balance to generate strong forces while avoiding unwanted contact between the coil and the magnet.

Time-varying currents create dynamic responses. For the case of vibrations, the amplitudes decrease with increasing frequency for motions in both normal and shear directions owing to a high damping ratio of the system, as shown in Fig. 2D and fig. S8. Amplitudes in the shear direction are typically larger than those in the normal direction, as the gap between the coil and magnet remains constant and coil does not interrupt the motion of the magnet in the shear case (movie S1). The FOM actuator can reproduce mixed forces, commonly encountered in practical, realistic scenarios, by

simultaneously engaging multiple coils. For instance, concurrent operation of the shear and normal coils generates a mixed shear and 25-Hz vibrational motion of the end effector (Fig. 2E and movie S2). The simultaneous operation of static shear and vibrations is essential to reproduce sensation of texture, as described subsequently (31). The control system, driven by a 32-kHz high-frequency clock, precisely regulates the ac voltage with a resolution of 100 μs (fig. S9), enabling the FOM actuator to achieve frequency resolution across all operational frequencies that exceeds the resolution of human perception (fig. S10).

Figure 2F presents the threshold currents required for human perception for various stimuli generated by FOM actuators on the dorsal hand. Tests of normal and shear stimuli, both static and dynamic (25 and 100 Hz), involve responses from 10 human subjects. Except for the static normal stimulus, the average threshold currents for all stimuli are <31 mA. Vibrations at 25 Hz are perceivable with a lower current than both static stimuli and 100-Hz vibrations. The corresponding threshold forces, ranging from 2.5 to 15 mN, are listed in table S3 and are comparable to the perceptual threshold forces reported in the literature (26, 32). While the perception threshold sets the minimum operational current, the temperature for safe operation on the skin defines the upper limit. The temperature of the actuator depends on the magnitude of the applied current, the coil resistance, the operational duration, and the duty cycle, as shown in Fig. 2, G and H, and fig. S11.

In an array configuration, the electromagnetic fields from neighboring actuators may interact, depending on their magnitudes and spacing (Fig. 2I and fig. S12). Simulations and experiments indicate that for spacing of 5 mm or more, electromagnetic interference is negligible. Environmental conditions, such as temperature, humidity, sweat secretion, and external load, do not significantly influence the performance of the actuator (Fig. 2J and figs. S13 and S14). Skin deformation around the actuators can affect the vibrations of the magnet by altering the dynamic system, caused by changes in effective skin modulus under deformed skin conditions (Fig. 2J). Specifically, compressive deformations can increase the vibrational amplitude through mechanical instabilities that lead to buckling of the skin. In contrast, tensile deformations can reduce the vibrational amplitude owing to the tension on the skin (fig. S15).

An extension of these ideas involves two sets of planar and normal coils, with the capability to generate normal, shear, and torsional forces across an array of four separate magnets (fig. S16). This design is beneficial in scenarios where there is a need for inducing three stimuli (normal, shear, and torsion) at a single point.

Human perception—haptic information transfer and encoding daily interactions

The capabilities of the FOM actuator platform allow not only for the replication of everyday tactile experiences but also for the transfer of information through programmed activation of mechanoreceptors in the skin. A goal is in identifying the specific nature of a sensory stimulus, which involves a comprehensive perceptual process that is much more complex and subtle than simply determining the presence or absence of a stimulus (33). The direction of mechanical stimuli is an intuitive physical parameter that can extend perceptual dimensionality and enhance information transfer (19), particularly when paired with other parameters related to the stimulation, such as frequency, intensity, rhythm, and location (single or multiple) (Fig. 3A). The studies reported here involve 12 distinct stimuli, combining direction and frequency, evaluated on the fingertip. The experiments include five static forces (normal and four orthogonal shear directions), vibrations along three axes at frequencies of 10 and 50 Hz, and a control condition with no stimulation. The results of tests with 10 human subjects indicate an ability to identify 96 applied stimuli with an average success rate of 88% (Fig. 3B). This corresponds to an information transfer (IT) value of 2.8 bits, achieved by a single actuator without relying on variations in intensity or spatiotemporal patterns (movement illusions) that are commonly used to enhance IT in haptic interfaces (34). The result, in comparison to other haptic interfaces, enables a high IT per actuator with a reduced dimensionality (fig. S17 and table S4). Reductions in the required numbers of actuators and the perceptual dimensions needed to achieve a given task improve wearability and energy efficiency, and they also minimize perceptual complexity. The variation in success rate for each stimulus (Fig. 3C) indicates no correlation with specific parameters; rather, it suggests considerable individual differences in the ability to identify stimuli, with individual IT values ranging from 2.64 to 3.53, as shown in fig. S18. Certain outliers with low success rates reflect failures in memory or in associating the stimulus with its correct name. Details on perception of multidirectional forces for various displacements, body locations, and other parameters are provided in fig. S19.

Arrays of FOM actuators can also replicate realistic sensations. Actuation at multiple points with appropriate spacing and relative timings can induce unified perceptions influenced by the concentration and receptive fields of mechanoreceptors in specific areas of the human body (35). The results in Fig. 3D demonstrate that the two-point discrimination thresholds (2PDTs) of shear forces in the same direction are 9.1, 28.8, and 50.3 mm at the fingertip, back-hand, and forearm, respectively. These values are

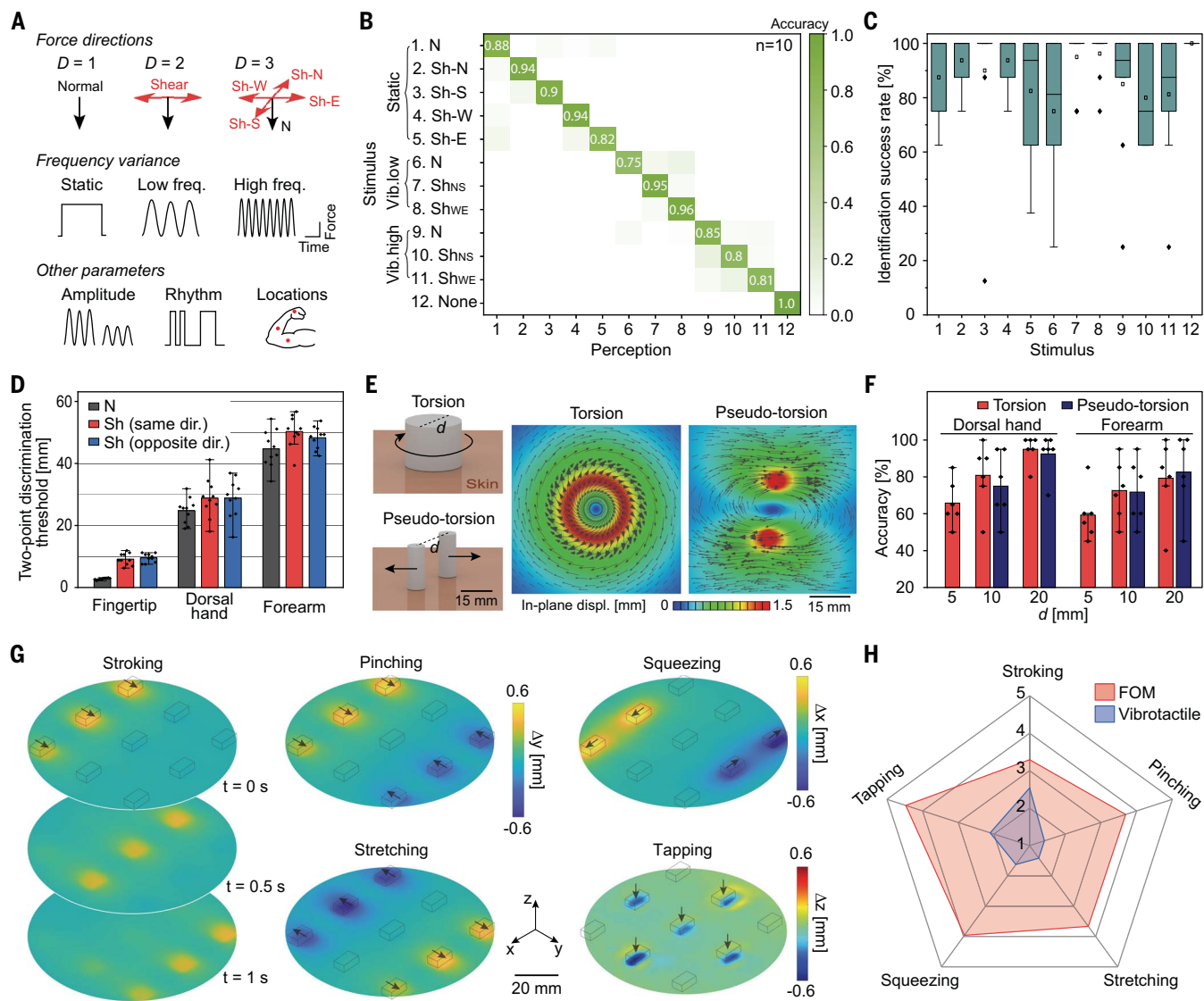


Fig. 3. Perception from FOM actuators. (A) Physical parameters of mechanical stimuli that support enhanced perceptual dimensions. (B) Accuracy in discriminating 12 mechanical stimuli applied by a single FOM transducer on a fingertip. (C) Variance in the success rate for identifying each stimulus. (D) Two-point discrimination threshold for normal, shear, and opposite shear forces on a fingertip, the dorsal hand, and the forearm. (E) Illustration of the application of torsion and pseudo-torsion on skin with corresponding simulations of the resulting deformations. (F) Success rate for directional perceptions of torsion

and pseudo-torsion for different contact diameters [d specified in (E)] on the dorsal hand and forearm. (G) Representations of displacements evaluated by digital image correlation with a skin phantom and a 3-by-3 FOM actuator array programmed to encode various mechanical interactions: stroking, pinching, stretching, squeezing, and tapping. (H) Human perception for the appropriateness of the five different stimuli generated by FOM and vibrations: 5, appropriate; 4, nearly appropriate; 3, reminds of appropriateness; 2, confused appropriateness; and 1, unrelated. The plotted values represent an average of eight results.

slightly larger than those observed for normal forces in our experiments (6.4, 4, and 5.6 mm, respectively) and in previous studies (table S5). This difference may be attributed to the comparatively large areas of skin deformation (fig. S20) for the case of shear forces and the larger receptive fields of the corresponding mechanoreceptors (13, 36). Opposing shear forces, which exhibit similar 2PDT values with the same directional shear, produce circular deformations of the skin that mediate a torsional perception, as an additional, distinct perceptual mode (Fig. 3E). Although pseudo-torsion gen-

erated by two opposite shears is mechanically different from true torsion, the perceptions of torsional direction relative to diameter are almost identical, as shown in Fig. 3F. This observation suggests that nested tri-coil FOM actuators in an array configuration can provide torsional perception.

Arrays of FOM actuators with spacing smaller than the 2PDT values can reproduce complex spatiotemporal stimuli, for everyday tactile experiences such as stroking, pinching, stretching, squeezing, and tapping (Fig. 3G and movie S3). Experimentally measured deforma-

tions of a skin phantom induced by operation of a 3-by-3 array of actuators demonstrate stimuli with distinct directions, areas, and timings for each sensation. The stimuli generated by FOM actuators produce more-realistic perceptions in humans than vibrotactile stimuli, which have been widely used in recent haptic applications (Fig. 3H and fig. S21). In a perception test where subjects rated the appropriateness of the stimuli reproduced by FOM and vibrations on a scale from 1 (unrelated) to 5 (appropriate), subjects found FOM stimuli to be more appropriate than vibrations for all types of stimuli.

Navigating hand positions with a single FOM actuator

Haptic interfaces can provide navigational or other inputs to individuals with visual impairments, of interest as a secondary sensory system without manual encumbrances or interferences with their primary hearing ability. Direct transfer of directional information with traditional haptic actuators requires arrays, which increases the overall size of the system. By contrast, the

multimodal operation of the FOM actuator and its use with the integrated IMU described previously avoids this requirement, to provide effective information with real-time adaptation to changing body orientation. In a demonstration, a person wearing smart glasses reaches to grasp a bottle and a granola bar, guided by an FOM actuator placed on the dorsal hand (Fig. 4A and movie S4). A smartphone that shares the view with the smart glasses recognizes the po-

sitions of the hand and target objects and sends commands to the FOM actuator. When the visual data include in-depth information, such as from a depth-sensing camera or dual camera, the navigating system can provide more-detailed guidance (movie S5). The same command generates different haptic stimuli depending on the hand position, which serves as a perceptual reference coordinate. For example, the command to move the hand upward translates to

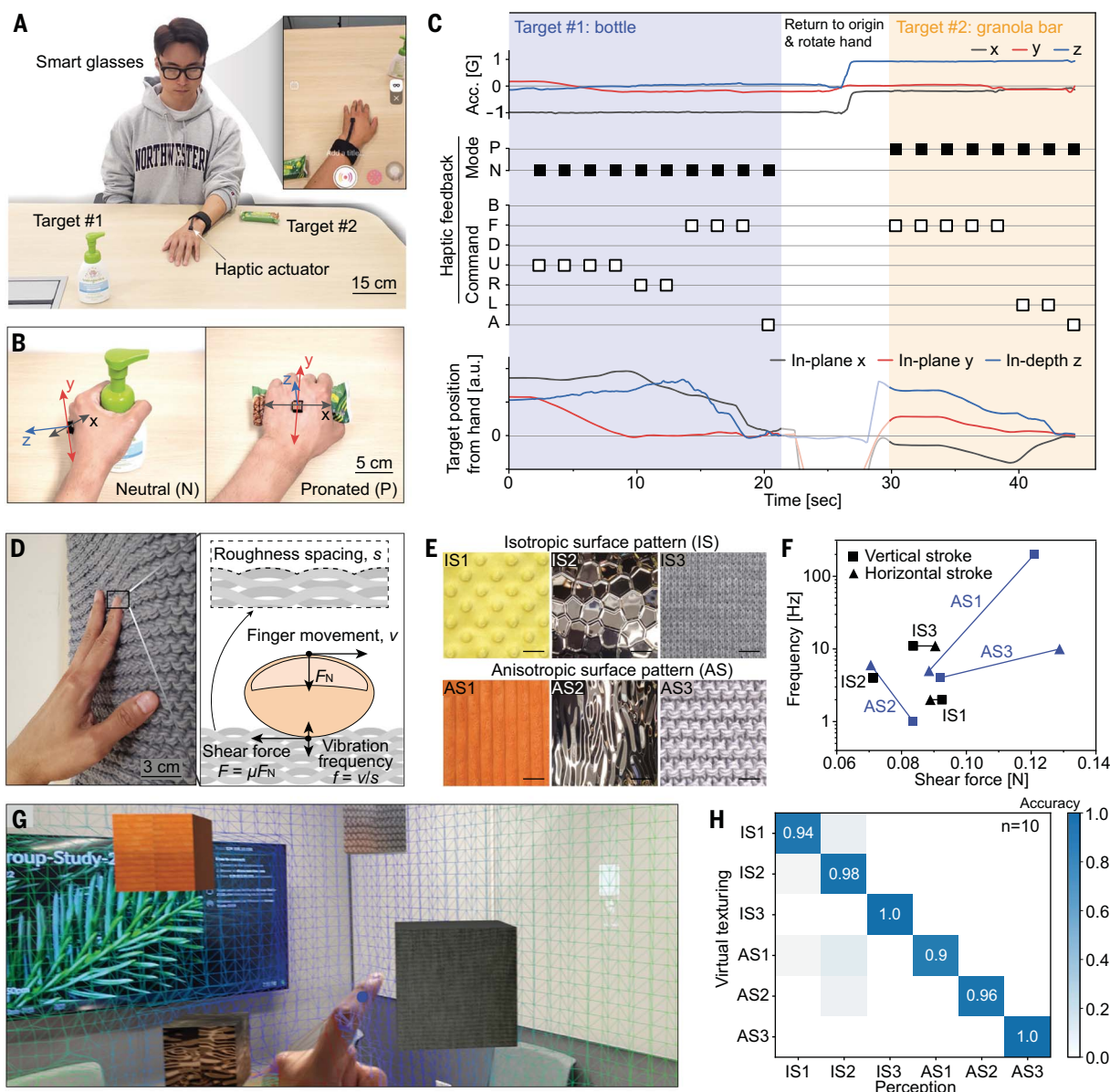


Fig. 4. Hand navigation system and reproduction of realistic textural sensations enabled by FOM actuators. (A) Photograph of a system for hand navigation based on a single FOM actuator. The inset photograph displays the corresponding view from the smart glasses. (B) Illustration of adaptation of the perceptual coordinate system depending on posture of the hand while grasping various items, enabled by outputs from the integrated IMU. (C) Data associated with haptic feedback during navigation to grasp two items: acceleration measured by the IMU, estimated hand posture on the basis of IMU data, haptic stimulus, and relative position of the target object from the hand based on data from a depth-sensing camera.

P, pronated; N, neutral; B, back; F, forward; D, down; U, up; R, right; L, left; A, arrive. (D) Photograph of tactile engagement with a fabric, accompanied by a schematic illustration of the dynamics of the fingertip while stroking. (E) Examples of various textile and metal surfaces with isotropic and anisotropic features of surface relief and mechanical properties. Scale bars, 2 cm. (F) Vibration frequencies and static shear forces that create realistic virtual textural sensations, depending on the surfaces and stroke directions. (G) Photograph of an XR display as a user experiences the texture of virtual objects. (H) Confusion matrix that illustrates the ability to differentiate various surfaces on the basis of the haptic stimulus.

positive x -directional haptic stimuli for a neutral hand posture, while it converts to positive z -directional stimuli for a pronated hand (Fig. 4B). The IMU in the actuator measures gravitational acceleration and determines the hand posture to issue the appropriate command. Figure 4C shows the measured acceleration, determined hand modes, haptic commands, and target positions during the demonstration. Movies S4 and S5 show that the individual successfully locates the bottle and granola bar using this form of haptic navigation.

Reproducing realistic virtual texture sensations using an array of FOM actuators

Realistic tactile sensations can represent essential aspects of an immersive experience in XR. Responses to surface textures result from complex patterns of deformation of the skin, where extension, compression, and vibration are key components (37). Limitations of traditional haptic actuators in this context follow from their inability to generate shear forces or torques or to mix these with normal forces in a fast, dynamic manner.

The FOM actuators can reproduce realistic texturing sensations on the fingertips when exploiting information from the IMU on the direction and speed of motion of the finger. Figure 4D and fig. S10 illustrate the connection between the material properties, morphologies, and mechanical characteristics of the finger and the

shear forces and vibrational frequencies that appear at the surface of the fingertip. Specifically, shear forces at the surface of the skin are proportional to the product of the friction coefficient between the skin and the target material and the normal force applied to the finger. Another key parameter for texture perception is vibration, with frequency determined by the spatial frequencies of roughness on the target surface and the finger and the speed of finger stroking. Demonstration experiments focus on reproduction of tactile sensations associated with six different objects, including those with both isotropic and anisotropic patterns of relief as shown in Fig. 4E and characterized in Fig. 4F and fig. S22.

These object-specific parameters allow programmable control of an FOM actuator to produce a virtual sensation in XR (Fig. 4G). On the basis of virtual vertical and horizontal stroking patterns, subjects can differentiate these six different surfaces with a 96% success rate (Fig. 4H).

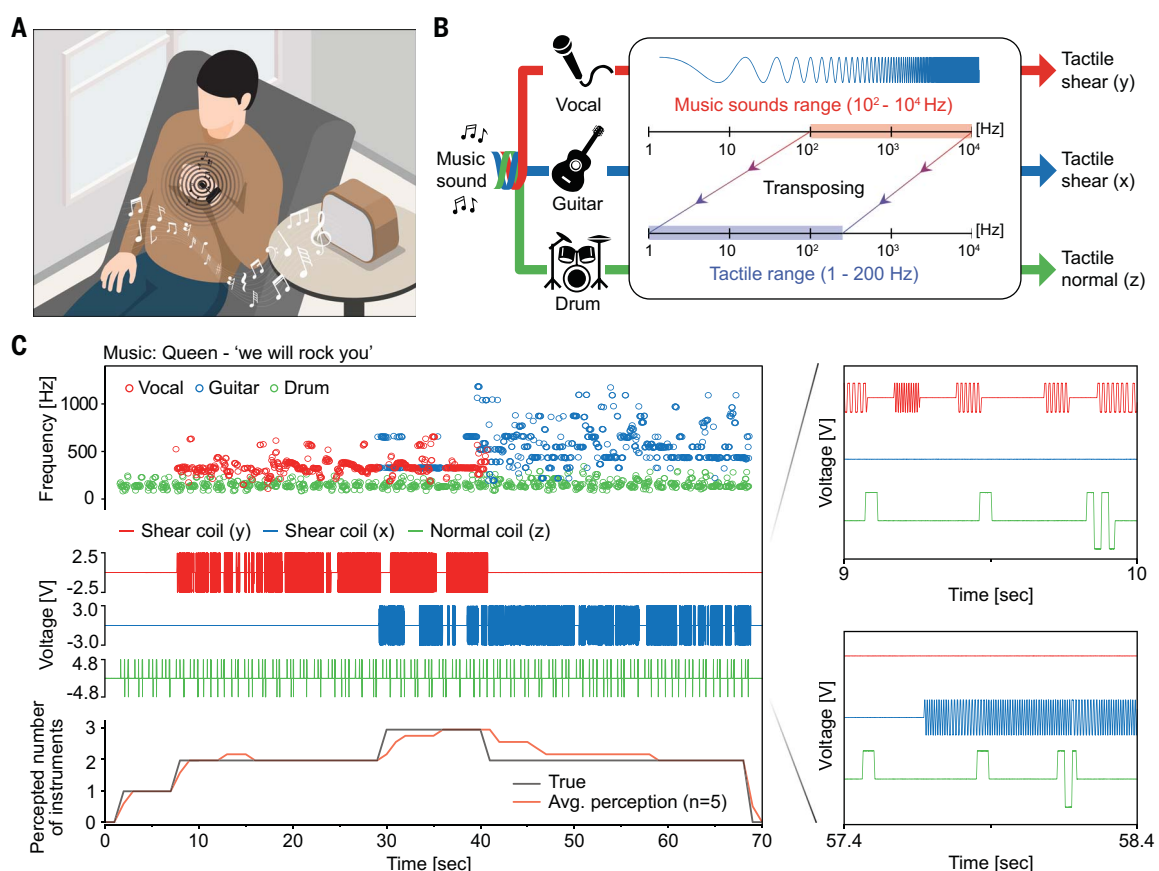
Experiencing music through haptic interfaces

Haptic interfaces, as a substitutional sensory system, provide an opportunity for individuals with hearing impairments to experience music; additional interest lies in enhancing these experiences for those without impairments (Fig. 5A). Physical properties of sound waves, such as frequency and intensity, can be intuitively converted into tactile vibrational forces provided by the FOM actuator platform, through appropriate range control (37). A challenge in transposing sounds to haptic sensations is in reproducing distinct tone quality, which corresponds to timbre. Despite identical frequencies, sounds from different musical instruments have different timbre. The FOM actuator can produce various quality vibrations by using directional control, in a way that cannot be reproduced with conventional actuators. This capability enables a single FOM actuator unit to replicate music comprising different musical instruments.

Figure 5B illustrates the process flow for converting music into haptic vibrations. The first step isolates each instrument and vocal component using a machine learning–based algorithm, to allow physical parameters (frequency and intensity) of each sound to be analyzed. The analyzed audio frequencies, within the audible range of 10^2 to 10^4 Hz, are transposed into the perceivable vibrotactile frequency range of 1 to 200 Hz for use in haptic interfaces. In the third step, these frequencies and corresponding intensities convert into time-varying voltage applied to different coils, and thus vibrational directions, for different instruments.

An illustration of this scheme involves conversion of a sample piece of music consisting of voice, electric guitar, and drums into a haptic

Fig. 5. Substitutional sensing: Tactile perception of music. (A) Illustration of a person perceiving music through tactile sensations. (B) Schematic diagram of the representation of music by means of distinct tactile stimuli corresponding to different musical instruments. (C) Auditory frequencies of various instruments and the corresponding voltages applied to each coil in the FOM device generate haptic sensations, allowing human subjects to recognize the number of instruments being played solely on the basis of haptic perceptions. Inset plots display the voltage signals over short time intervals.



interface (movie S6). Figure 5C depicts the extracted frequencies of the vocal, guitar, and drums, along with the corresponding voltages applied to the coils. The right panels in Fig. 5C show the alternating voltages with varying frequencies at two time intervals on three coils. Perception tests confirm the ability to feel distinct tones of vibrations and to recognize a mixed collection of instruments by haptic interfaces conveyed through a single actuator.

Conclusions

The miniaturized, skin-integrated haptic actuator platforms introduced here are distinguished by their ability to deliver omnidirectional, superimposable, static and dynamic forces to the surface of the skin. This operation allows for programmable stimulation of various cutaneous mechanoreceptors, individually or in combination, as an essential aspect of future immersive XR experiences. Wireless, real-time operation, either as single units or as arrays distributed on desired body parts, yields various types of perceptible sensations in an efficient manner. Complete experimental and theoretical work identifies the physics of multicoil electromagnetics, including a validated analytical model that guides optimized choices in designs for compact, efficient operation. In comparison to conventional haptic interfaces, these technologies enable high-bit haptic information transfer and virtual tactile sensations with enhanced realism. Human perception tests and representative use cases highlight additional features. The latter include hand navigation for the visually impaired, textural sensation through mixed forces, and sensory substitution for music perception, all of which can be achieved with one or multiple actuators under closed-loop control by acoustic or motion feedback. Building on the FOM operation technology introduced in this work, future efforts may establish routes for further reducing the dimensions and the

effective modulus of the FOM actuator for high-density, conformable haptic interfaces (figs. S23 to S25). The development of in-plane coil structures or related configurations, suitable for lithographic fabrication, may offer additional benefits in miniaturization.

REFERENCES AND NOTES

- A. Zimmerman, L. Bai, D. D. Ginty, *Science* **346**, 950–954 (2014).
- W. Lin et al., *Sci. Adv.* **8**, eabp8738 (2022).
- Y. H. Jung et al., *Nat. Electron.* **5**, 374–385 (2022).
- X. Yu et al., *Nature* **575**, 473–479 (2019).
- E. Leroy, H. Shea, *Adv. Mater. Technol.* **8**, 2300242 (2023).
- J. Yin, R. Hinchet, H. Shea, C. Majidi, *Adv. Funct. Mater.* **31**, 2007428 (2021).
- Y. H. Jung, J. H. Kim, J. A. Rogers, *Adv. Funct. Mater.* **31**, 2008805 (2021).
- E. Abdi, D. Kulić, E. Croft, *IEEE Trans. Biomed. Eng.* **67**, 3438–3451 (2020).
- J. Bimbo, C. Pacchierotti, M. Aggravi, N. Tsagarakis, D. Prattichizzo, in *2017 IEEE/RSJ International Conference on Intelligent Robots and Systems (IROS)* (IEEE, 2017), pp. 3401–3408.
- Y. S. Choi et al., *Science* **376**, 1006–1012 (2022).
- P. B. Shull, D. D. Damiani, *J. Neuroeng. Rehabil.* **12**, 59 (2015).
- M. T. Flavin et al., *Nature* **635**, 345–352 (2024).
- G. Corniani, H. P. Saal, *J. Neurophysiol.* **124**, 1229–1240 (2020).
- A. Handler, D. D. Ginty, *Nat. Rev. Neurosci.* **22**, 521–537 (2021).
- B. Delhyae, A. Barrea, B. B. Edin, P. Lefèvre, J.-L. Thonnard, *J. R. Soc. Interface* **13**, 20150874 (2016).
- N. L. Neubarth et al., *Science* **368**, eabb2751 (2020).
- S. Guest et al., *Atten. Percept. Psychophys.* **73**, 531–550 (2011).
- J. Turecek, B. P. Lehnert, D. D. Ginty, *Nature* **612**, 310–315 (2022).
- K. T. Yoshida et al., *IEEE Trans. Haptics* **17**, 483–495 (2024).
- M. Sarac et al., *IEEE Robot. Autom. Lett.* **7**, 6099–6106 (2022).
- S. R. Williams, J. M. Suchoski, Z. Chua, A. M. Okamura, *IEEE Robot. Autom. Lett.* **7**, 3310–3317 (2022).
- Z. Zhakyrov, A. M. Okamura, in *2022 IEEE 5th International Conference on Soft Robotics (RoboSoft)* (IEEE, 2022), pp. 938–944.
- M. Zhu et al., in *Proceedings of the 2020 CHI Conference on Human Factors in Computing Systems* (Association for Computing Machinery, 2020), pp. 1–12.
- P. Zhang, M. Kamezaki, Y. Hattori, S. Sugano, in *2022 International Conference on Robotics and Automation (ICRA)* (IEEE, 2022), pp. 8869–8875.
- N. A.-h. Hamdan, A. Wagner, S. Voelker, J. Steimle, J. Borchers, in *Proceedings of the 2019 CHI Conference on Human Factors in Computing Systems* (Association for Computing Machinery, 2019), pp. 1–14.
- E. Leroy, R. Hinchet, H. Shea, *Adv. Mater.* **32**, e2002564 (2020).
- J. Wan et al., *Sci. Adv.* **10**, eadm9314 (2024).
- Y. Luo et al., *Nat. Commun.* **15**, 868 (2024).
- Y. Huang et al., *Nat. Electron.* **6**, 1020–1031 (2023).
- A. Kaneko, N. Asai, T. Kanda, *J. Hand Ther.* **18**, 421–425 (2005).
- Z. Liu, J.-T. Kim, J. A. Rogers, R. L. Klatzky, J. E. Colgate, *IEEE Trans. Haptics* **17**, 441–450 (2024).
- S.-A. Abad, N. Herzig, D. Raith, M. Koltzenburg, H. Wurdemann, *Nat. Commun.* **15**, 7631 (2024).
- M. W. Brown, J.-Z. Xiang, *Prog. Neurobiol.* **55**, 149–189 (1998).
- H. Z. Tan, S. Choi, F. W. Lau, F. Abnousi, *Proc. IEEE* **108**, 945–965 (2020).
- C. Pasluosta, P. Kiele, T. Stieglitz, *Clin. Neurophysiol.* **129**, 851–862 (2018).
- Y. Roudaut et al., *Channels (Austin)* **6**, 234–245 (2012).
- M. D. Fletcher, *Front. Neurosci.* **15**, 723877 (2021).

ACKNOWLEDGMENTS

The authors thank Y. Wang for preliminary assistance in fabricating devices. **Funding:** This work was funded by the Querry-Simpson Institute for Bioelectronics. J.Y. acknowledges funding from the Basic Research Laboratory (BRL) Project from the National Research Foundation (RS-2024-00406674) funded by the Ministry of Science and ICT of Korea, as well as the Technology Innovation Program (RS-2024-00443121) funded by the Ministry of Trade, Industry and Energy (MOTIE, Korea). **Author contributions:** Conceptualization: K.-H.H., J.A.R.; Formal analysis: K.-H.H., S.L., Y.M., S.X., H.Q., H.W., C.F., H.Y., P.S., S.K., E.C.; Funding acquisition: Y.H., J.A.R.; Investigation: K.-H.H., J.Y., S.L., Y.M., S.X., H.Q., H.W., C.F., H.Y., J.-T.K., P.S.; Methodology: K.-H.H., J.Y., S.L., Y.M., M.T.F., E.C.; Project administration: Y.H., J.A.R.; Software: K.-H.H., J.Y.; Supervision: K.-H.H., Y.H., J.A.R.; Validation: K.-H.H., Y.M., S.X.; Visualization: K.-H.H., J.Y., S.L., Y.M., S.X., H.Q., H.W., C.F., H.Y., J.-T.K., S.Y.; Writing – original draft: K.-H.H.; Writing – review & editing: K.-H.H., J.Y., S.L., Y.M., H.Q., H.-Y.A., Y.H., J.A.R. **Competing interests:** The authors declare that they have no competing interests. **Data and materials availability:** All data are available in the main text or the supplementary materials. **License information:** Copyright © 2025 the authors, some rights reserved; exclusive licensee American Association for the Advancement of Science. No claim to original US government works. <https://www.science.org/about/science-licenses-journal-article-reuse>

SUPPLEMENTARY MATERIALS

science.org/doi/10.1126/science.adt2481

Materials and Methods

Supplementary Text

Figs. S1 to S29

Tables S1 to S8

References (38–68)

Movies S1 to S6

Submitted 18 September 2024; accepted 14 February 2025
[10.1126/science.adt2481](https://science.org/10.1126/science.adt2481)